Development of an auto-tuning magnet girder with high stability and accuracy

Haijing Wang[1,*], Zihao Wang[1], Chunhua Li[1,*], Jia Liu[1], Hongyan Zhu[1, 2], Huamin Qu[1]

[1]Institute of High Energy Physics, Chinese Academy of Sciences, 100049, Beijing, China

[2]Lawrence Berkeley National Laboratory, 1 Cyclotron Road, Berkeley, CA94720, U.S.

Abstract: With the development of high-performance photon sources which have extremely low emittance, auto-tuning magnet girder has drawn more and more attention, especially for the diffraction-limited storage rings and free-electron lasers. The biggest challenge is to simultaneously obtain high stability and high flexibility. In this paper, an auto-tuning magnet girder prototype has been designed and developed. The topological optimization, multi-point supports and locking systems have been applied for magnet girder design to improve the stability. The modal analysis accords with the vibration test well. The natural frequency of the magnet-girder assembly is deduced as high as 45.6 Hz, which demonstrates good stability. Ball-cam movers have been chosen as adjustment mechanisms and closed loop control scheme has been used to pursue high accuracy. The kinematic resolution is better than 1 μm, and the accuracy is better than 1 μm within the adjusting range of ±5 mm. Besides, it can eliminate most of the calibration which can save much manpower and time. The tests demonstrate that the magnet girder can be used for beam-based girder alignment with high stability and high accuracy.

I. INTRODUCTION

The extremely high brilliance and low emittance is becoming an urgent need with the study and development of the photon sources, especially for the DLSRs (diffraction-limited storage rings) and FELs (free-electron lasers) [1]. Almost all new-designed or upgraded synchrotron radiation photon sources have the requirements of the emittance at sub-nm level or even lower, for example, 42 pm.rad for APS-U [2], and 34 pm.rad for HEPS [3-4]. It is necessary for the magnets to have ultrahigh stability and alignment accuracy simultaneously, which brings great challenge to the magnet girders design.

Vibration and motion of the lattice elements can lead to significant beam emittance growth and brilliance degradation. The former occurs mainly at frequency above 1Hz and can be improved by stable girders, beam-based feedback system and so on. While the latter is slow position drift necessitates re-alignment, for which the flexible and accurate kinetic mechanism is preferred.

The natural frequency is an important parameter for stability because of the rapid drop in ground vibration amplitude at higher frequencies, which can be seen at APS [5], HEPS [6] and other different accelerator sites [7], although the values are strongly site dependent. The natural frequency and misalignment tolerance of some new-designed or updated photon sources are listed in Table I. Except the Sirius which adopts small and light girders to achieve a much higher natural frequency, most of other facilities use relatively long girders. Almost all the new synchrotron radiation photon sources chose the non-automatic or semi-automatic adjusting mechanisms such as wedge jacks to obtain the high magnet stability. TPS used the ball-cam movers for the automatic alignment. The price is that the required natural frequency was higher than 30Hz and the tested number was 33Hz with locking system, lower than the other facilities.

*Corresponding authors.

wanghaijing@ihep.ac.cn (H. Wang), lichunhua@ihep.ac.cn (C. Li)

Table I. Requirements on magnet girders of some new-designed or updated photon sources

Facility	Natural frequency requirements (Hz)	Misalignment tolerance (μm)	Adjusting method
HEPS	≥54	≤50	Wedge jacks
APS-U (Ref. [8])	≥50	≤100	Manual
Sirius (Ref. [9])	152 (Tested)	≤80	
ESRF-EBS (Ref.	≥35	≤50 (Vertical-transv.)	Wedge jacks
[10])	51 (Tested)	≤1000 (Longitudinal)	Semi-automatic
TPS (Ref. [11])	≥30	≤100	Ball-cam movers
	33 (Tested)		Automatic

The misalignment tolerance between girders can reach 50 μm by using laser tracker and accurate wedge jacks, and can be hardly improved further. The auto-tuning girder is an essential and urgent challenge for the beam-based girder alignment owing to the good adjusting flexibility and accuracy. It may take over most of the static orbit correction and leave the corrector strength to dynamic correction (active orbit feedback) and local bump creation for matching to beamline acceptances or for machine studies [12]. The existing auto-tuning magnet girders mainly use ball-cam mover as the kinetic mechanism, which was first applied in the Final Focus Test Beam (TTFB) at SLAC [13], and then adopted in some photon sources, such as SLS [12], Diamond [14] and TPS [11]. The mechanisms of SLS and Diamond are similar, using five ball-cam movers to adjust five degree of freedoms (translation along beam direction excluded). TPS has improved the design to adjust the six degree of freedoms. Based on which, the position of the girder can be totally controlled. The auto-tuning girder can reach better position accuracy and save much manpower and time, while it is very hard to reach high natural frequency, for example, above 50 Hz, as listed in Table II.

Table II. Performance of existing auto-tuning magnet girders

Facilities	FFTB (Ref. [8])	SLS (Ref. [15-16])	TPS (Ref. [11, 17 18])
Natural frequency (Hz)	N/A	16	33
Adjusting range (mm)	X/Y: -1.19~0.32	X/Y:＜±3.5	X: ±4.5, Y: ±9, Z: ±7
Resolution (μm)	0.4	3	0.03 (deduced)
Accuracy (μm)	Not locked: ≤5	Not locked: ≤5	Not locked: ≤10 Locked: X: ≤10, Y/Z: not controllable
Necessity of main dimension calibration	Yes	Yes	Yes

The stability has positive correlation with the support stiffness, which needs larger contact area and locking forces. While the flexibility calls for the kinetic mechanism with appropriate constraints and less interference such as friction. The requirements of high stability and high flexibility conflict with each other to some extent. Therefore, it is difficult to handle both. Using locking system after adjustment is a practical method as used in TPS, while the uneven locking forces can bring a decreased alignment accuracy. It may be improved by locking system calibration to balance the force condition on the girder, or by fine-tuning with the locking forces.

The magnet girder design is a comprehensive consideration of magnet stability, adjustment accuracy and flexibility, convenient installation, lattice periodicity, cost and so on, among which the magnet stability, the adjustment accuracy and flexibility and the cost may be the most important factors. Many light sources didn't choose the auto-tuning magnet girders owing to the existing relatively lower stability as well as much higher costs. But as a technical research, auto-

tuning magnet girder with high stability and high accuracy has drawn more and more attention, pursuing the extremely high brilliance and low emittance.

In this paper, an auto-tuning magnet girder prototype has been developed with good performance. The natural frequency of the magnet-girder assembly is deduced as high as 45.6 Hz or even higher, which is comparable with the new-designed photon sources with manual wedge jacks. The adjusting ranges can be larger than ±10 mm with improved accuracy of better than 1 μm and 5 μrad without locking system, and better than 8 μm and 15 μrad after locked.

II. STRUCTURE DESIGN

The girder prototype was designed corresponding to the straight multiplet of the HEPS-TF (Test facility of High Energy Photon Source) lattice design [19] which has nine magnets. It is composed of girder body, ball-cam movers, pedestals, locking systems, fake magnets (gravity loads), sensors and control system, as shown in Fig.1.

The girder body is 3300 mm long, which is welded with steel plates to reduce weight and improve manufacturability. The upper plate is 50 mm thick on which nine steel blocks weighting about 6.5 tons in total are mounted as fake magnets. Six ball units are mounted at the upper boundaries of the girder body, each of which matches with a cam mover mechanism correspondingly. The six cam movers are fixed on the top of three pedestals. The pedestals are also steel plate weldments which are designed to be fixed at the lower surface. Six locking systems are placed symmetrically between the girder body and the three pedestals, which are used to lock the girder body after adjustment to improve the natural frequency of the magnet-girder assembly. Similar to the design of TPS [17], each locking system includes a wedge block for locking, some disc springs for buffering and a motor-driven screw. There are eight length gauges to monitor the translation and rotation of the girder body. The gauge blocks are mounted to the girder body or pedestals and the measuring contacts are contacted the corresponding reference.

In this paper, X refers to horizontal direction, Y refers to vertical direction, Z refers to beam direction, Pitch refers to rotation along X-axis, Yaw refers to rotation along Y-axis, and Roll refers to rotation along Z-axis respectively.

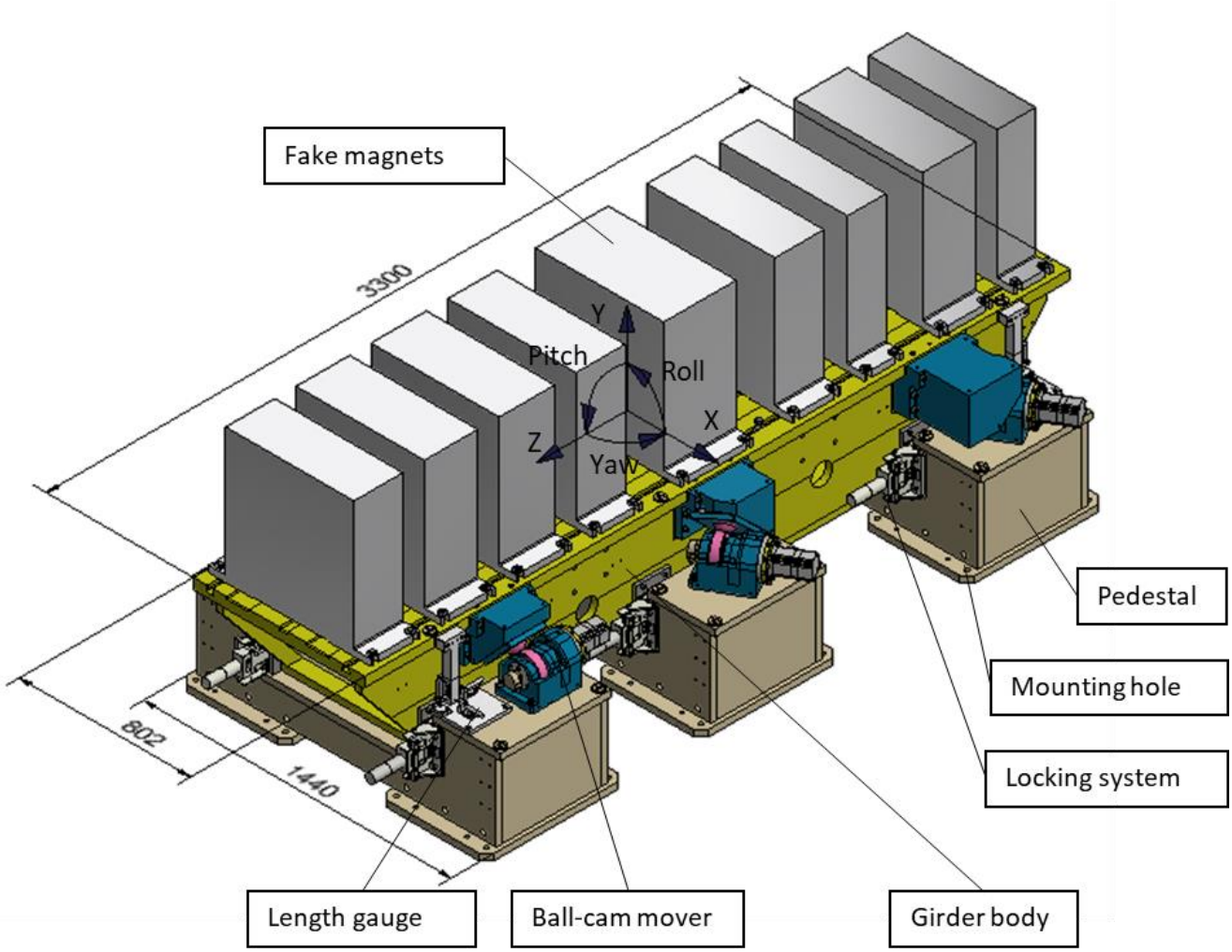

FIG. 1. Design sketch of the auto-tuning magnet girder prototype

III. STABILITY STUDY

A. Topological optimization of the girder body

Topological optimization has been first applied in this girder prototype design [20], which afterwards has been used in the girder design of APS-U and Sirius [8,21]. This method is to find the best use of material so that an objective criterion takes out a maximum or minimum value subject to given constraints. In our case, both static and dynamic topological optimizations have been analyzed for the girder body using ANSYS parametric design language (APDL) code. The aim of the static optimization is to minimize the compliance which indicates the highest static stiffness and minimum deformation. And the aim of the dynamic optimization is to maximum the natural frequency which indicates the highest dynamic stiffness.

The model for optimization is shown in Fig. 2. The six ball unit housings are set as fixed constraints, and the girder body except the upper plate is used for optimization. For the static optimization, the weights of magnets about 6.5 tons are set as force loads for faster calculation with smaller number of nodes. The single compliance is specified as the objective function. And 80% volume decrease of the initial value is specified as the constraint. For the dynamic optimization, the models of fake magnets are remained because they are important for the mass matrix, while other settings are similar to the static optimization.

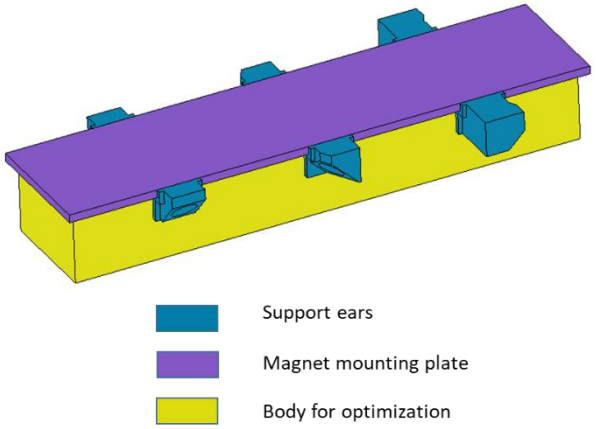

FIG. 2. Model for topological optimization

Both the static optimization and the dynamic optimization converge well. The static stiffness of the girder body plays a dominant role of the uneven flatness for the whole assembly, while the dynamic stiffness of that plays a relative weak role because of the even weaker stiffnesses of other components like the ball-cam movers. Thus, the result of the static optimization is mainly referred to, while the dynamic optimization is considered as supplement. The convergence curves and the distribution of element pseudo-density of static optimization are shown in Fig. 3. After optimization the deformation and the natural frequency have been highly improved, as listed in Table III.

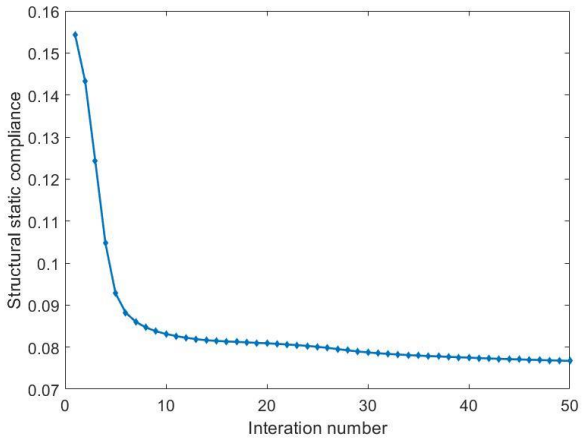

(a)

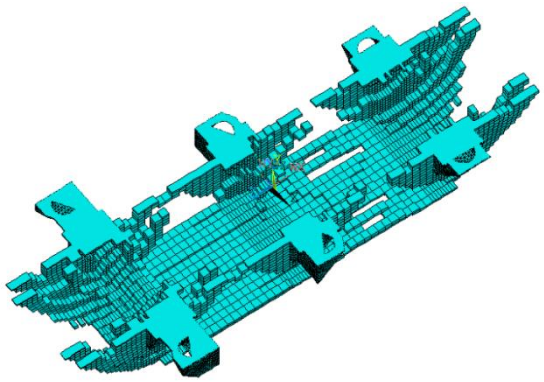

(b)

FIG. 3. Results of static optimization. (a) Convergence curve and (b) High pseudo-density elements

Table III. Improvements of the girder body before and after topological optimization

	Before optimization, solid block[a]	Before optimization, Frame[b]	After optimization
Weight (Kg)	8616	2114	2424
Max. uneven deformation (μm)	13.4	26.0	10.2
Natural frequency of girder body (Hz)	206.4	137.1	307.4

[a]Before optimization, the girder body is a solid block shown as Fig. 2.

[b]Before optimization, the girder body is welded by four plates without inner ribs.

B. Modal analyses and vibration test

The magnet-girder assembly can be considered as a multi-degree-of-freedom system, the differential equations of motion can be described as

$$M\ddot{\boldsymbol{X}} + C\dot{\boldsymbol{X}} + K\boldsymbol{X} = \boldsymbol{F}, \tag{1}$$

From which the natural circular frequency ω_p can be deduced from

$$\left|K - \omega_p^2 M\right| = 0, \tag{2}$$

where M is the mass matrix, C is the damping matrix, K is the stiffness matrix, $\boldsymbol{F}$ is the excitation force vector and $\boldsymbol{X}$ is the displacement vector.

The ball-cam movers can be considered as springs, the stiffness of which can be estimated by the force and deformation. The deformation of the ball-cam mover can be decomposed by several major factors, as shown in Fig. 4. D1 and D2 are the deformations at contact positions which can be calculated by Hertz theory [22]. D3 and D4 are the deformations from the bearings which can be calculated by empirical equations [23]. D5 is the deformation of the shaft and D6 is the deformation of elastic materials. The calculated deformations of each factor by gravity are listed in Table IV.

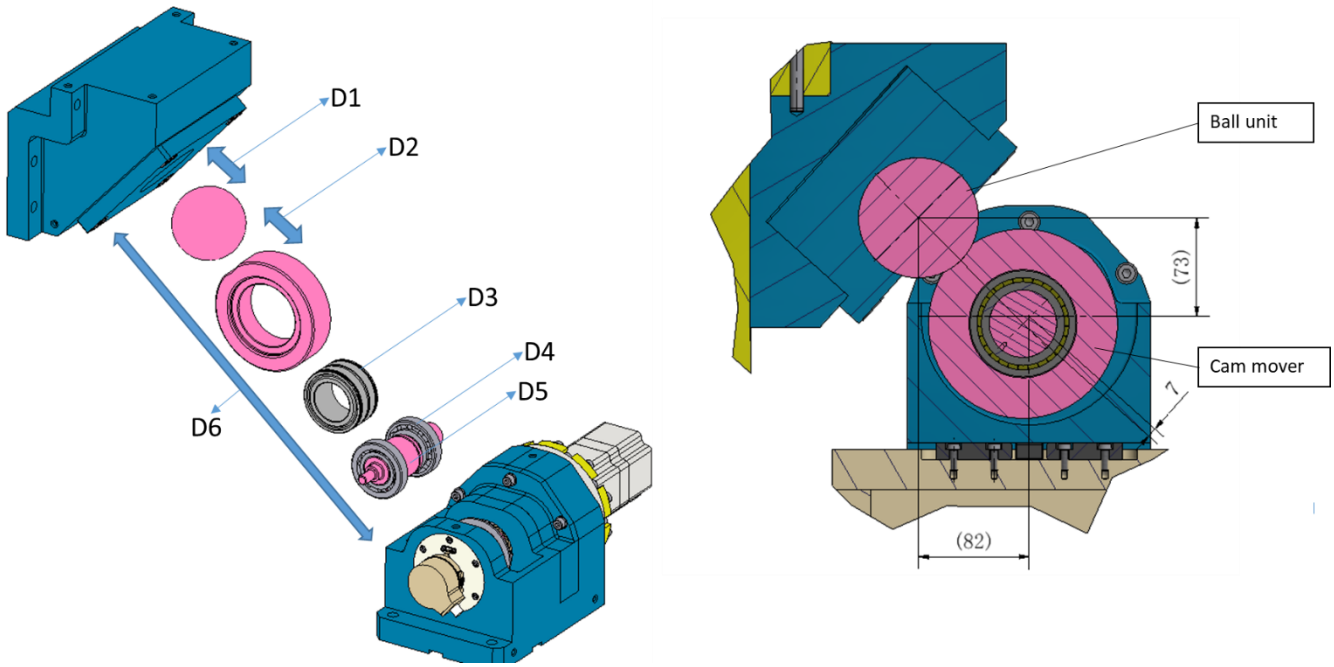

FIG. 4. Major factors of the deformation between ball unit and cam mover. (a) Exploded structure and (b) Cross section

Table IV. Calculated deformation by gravity of the ball-cam mechanism

Name	D1	D2	D3	D4	D5	D6	Total
Deformation (μm)	11	10	12	29	19	13	94
Source	Ball-housing contact	Ball-cam contact	Bearing	Bearing	Shaft	Elastic deformation	

Unlike the stiffness of the ball-came movers, the stiffness of locking system and that between the pedestal and ground are difficult to estimate, which obviously, cannot be considered as rigid joints. Three operation cases have been considered to study the roles of locking system and pedestal stability. FEM modal analyses using ANSYS as well as the experimental modal analysis have been done. In Case 1, the pedestals are fixed by anchor bolts and there are no locking systems. In Case 2, the pedestals are fixed by anchor bolts and there are six locking systems. And in Case 3, the pedestals are grouted to the ground and there are six locking systems. For these cases, the anchor bolts are at the mounting holes, while the locking systems are between the girder body and pedestals, as shown in Figure 1. In the tests, the pedestals are mounted to ground by anchor bolts only because grouting is not allowed in the experimental hall. But the natural frequency can be deduced if the calculated results of the first two cases accords with the tested results well, and in fact they do, as listed in Table V. The natural frequencies and modal shapes of the FEA results accords the tested results very well. Figure 5 shows the first-order mode shapes of FEA in the three cases, and Fig. 6 shows the tested mode shapes and transfer functions of Case 2.

Table V. Comparison between FEA results and tested results of the magnet-girder assembly[a]

		First-order mode (Hz)	Second-order mode (Hz)	Natural frequency of pedestals (Hz)
Case 1: pedestals fixed by anchor bolts and without locking systems	FEA	17.6 (X+Yaw)	18.8 (Z+Pitch)	FEA: 63.1 Hz
	Tested	17.3 (X+Yaw)	19.7 (Z)	Tested: 56.1 Hz
	FEA error	1.7%	4.6%	
Case 2: pedestals fixed by anchor bolts and with locking systems	FEA	25.5 (X)	27.2 (Z+Pitch)	FEA: 63.1 Hz
	Tested	24.4 (X)	27.0 (Z+Pitch)	Tested: 56.1 Hz
	FEA error	4.9%	0.7%	
Case 3: pedestals grouted to the ground and with locking systems	FEA	45.6 (X+Roll)	55.6 (Z+Pitch)	FEA: 190Hz
	Tested	---	---	Tested: ---

[a]The directions are defined in Section II. "X+Yaw" means the mode is a superposition with transition in X direction and rotation along Y-axis. And others in a similar fashion.

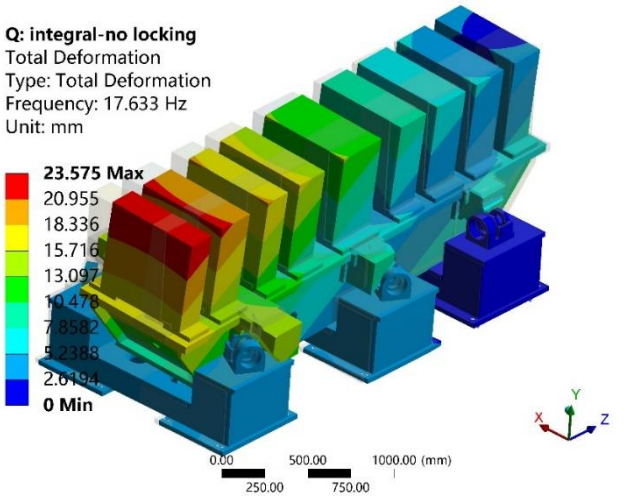

(a)

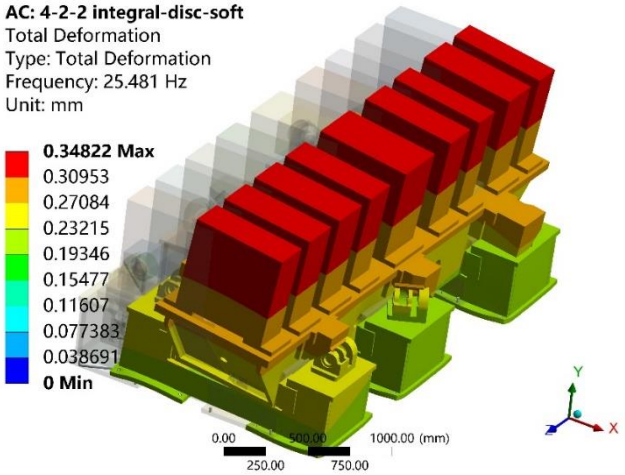

(b)

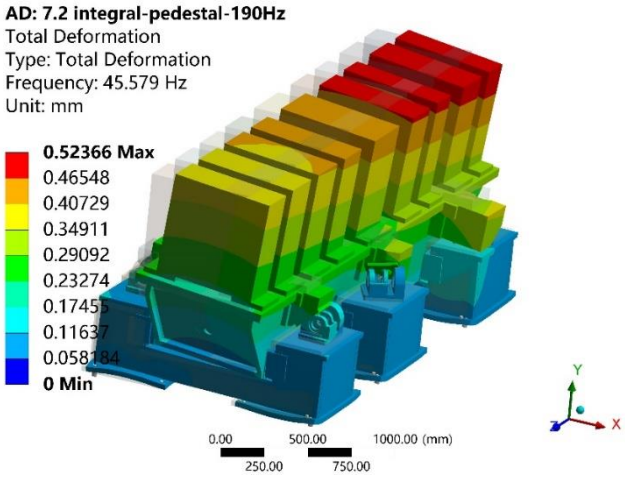

(c)

FIG. 5. First-order FEA mode shapes of the magnet-girder assembly prototype, in the cases of (a) case1, (b) case 2 and (c) case 3

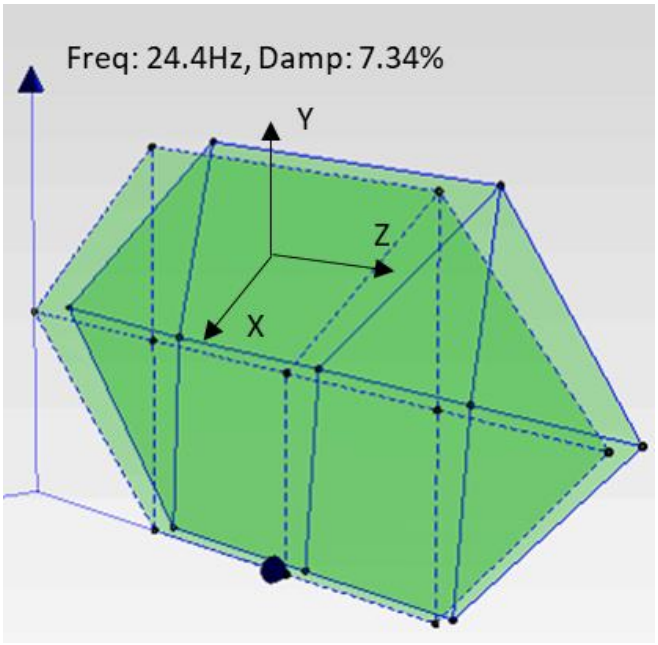

(a)

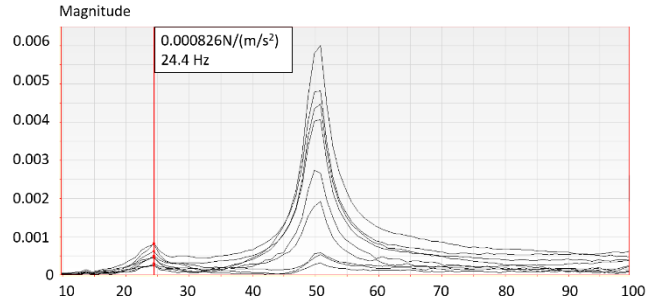

(b)

FIG. 6. Tested results of Case 2, (a) the first-order mode shape and (b) the transfer function of X-direction vibration

The tests demonstrate the locking system can improve the natural frequency definitely. The natural frequency of the assembly becomes higher with the increase of the locking forces and become constant when the locking forces are larger than 2 tons, which indicates that the contacts have been stabilized and the locking systems presented their own stiffnesses.

The stability of the pedestals also plays an important role to the assembly stability. The natural frequencies of the pedestals in Case 1 and Case 2 are the same, which are 56.1 Hz by testing and assumed 63.1 Hz in FEA. But it can be enhanced obviously if the pedestals were grouted to the ground. The natural frequency of grouted pedestal with similar dimensions can reach over 200 Hz in TPS [24] and 420 Hz in HEPS [25]. The analyzed natural frequency of the magnet-girder assembly can reach 45.6 Hz when that of the pedestal is 190 Hz, which can be even higher with higher stability of the pedestals.

Figure 7 shows the comparison of the harmonic responses in X direction of these three cases. The inputs are the harmonic nodal displacements at the same position of the earth under the pedestals, whose amplitude is 10 nm and frequencies are from 2 to 100 Hz. The response curves are recorded at the center of the magnet which is on the side of the girder. It is obvious that a lower natural frequency can lead to a larger vibration in the lower ground motion frequencies. Considering the higher ground vibration amplitude at lower frequencies, the vibration can be even worse. The responses in other directions are similar. And that's why the stabled girder with higher frequency is preferred for the photon sources and other similar facilities with DC magnets.

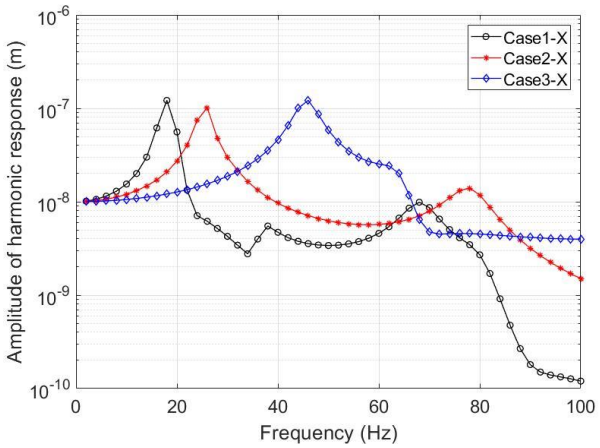

FIG. 7. Amplitude of harmonic response of the magnet on side of the girder

IV. KINETIC STUDY

A. Kinetic mechanism

For our prototype, ball-cam movers have been chosen as the kinetic mechanism for its high accuracy, compact structure and multi-degree of freedom. The theory of Boyes Clamp [26] is adopted as the kinematic support, which was also used in TPS [11]. Figure 8 (a) is the diagram, which shows a kinematic three-point footing can be used to define the upper body's position when the balls are mounted to the rigid upper body. The girder has six support points which can be considered as three pairs. Each pair can be assumed as a big and rigid ball, and the two corresponding shafts can be assumed as a groove, as shown in Fig. 8(b). then the position of the girder can be verified by these three assumed balls and their three assumed angled grooves. The grooves can be changed by rotating the cam shafts, then the position of the girder can be controlled.

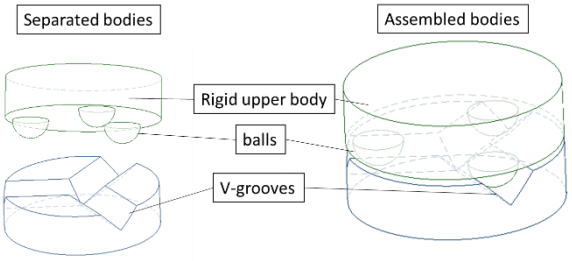

(a)

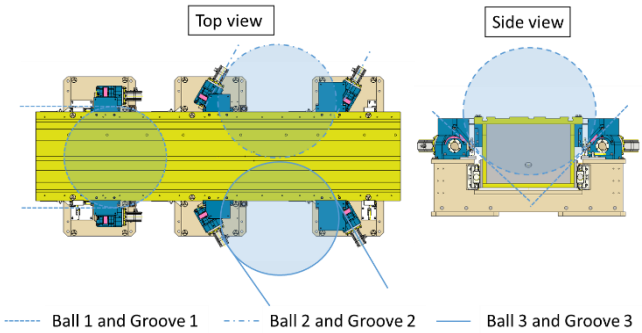

(b)

FIG. 8. Kinetic design principle of the prototype, (a) diagram of Boyes Clamp and (b) assumed balls and grooves

Figure 9 shows the diagrammatic drawing of one ball-cam mover. The main dimensions always fulfill the relation described as

$$d = \sqrt{(x + rcos(\theta + \varphi) - u)^2 + (y + rsin(\theta + \varphi) - v)^2}, \quad (3)$$

where d is the center-to-center distance of the ball and the cam, x and y are the origin relative positions between the ball and the cam in the two directions, u and v are the adjusting values of the ball in two directions, r is the eccentricity of the cam center and the fixed axis, θ is the starting angle of the cam and φ is the adjusted angle.

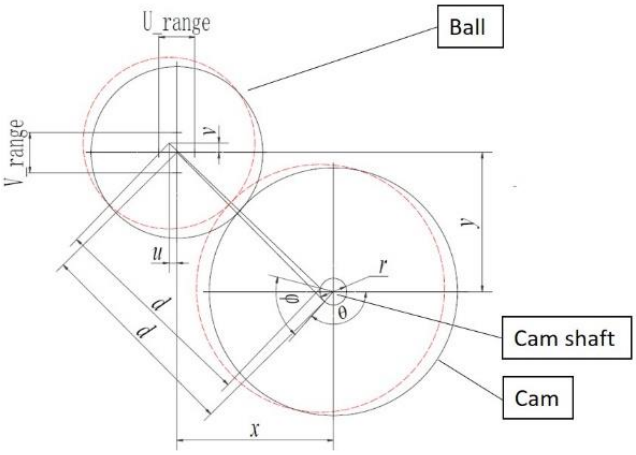

FIG. 9. The diagrammatic drawing of one ball-cam mechanism

The values d=110 mm, x=82 mm and y=73 mm are chosen based on optimization using MATLAB codes to achieve large and symmetrical adjusting ranges. The requirements of the adjusting ranges are ±8 mm in horizontal direction and ±10 mm in vertical direction, in consideration of processing tolerance, uneven ground and long-term position drift. Neglecting the machining and assembly errors, the adjusting ranges of each mechanism are from -9.43 mm to 9.33 mm in horizontal direction and from -10.67 mm to 10.46 mm in vertical direction, respectively, as shown in Fig. 10. Then the adjusting ranges of the girder can be induced by simple coordinate transformation and the Pythagorean theorem. Open-loop tests with dial indicators are done to verify the adjusting ranges, as listed in Table VI. The position targets in the tests are about 1 mm less than the calculated ones for safety consideration.

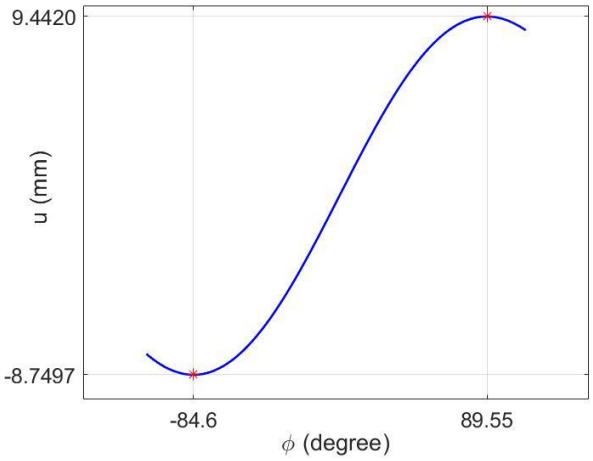

(a)

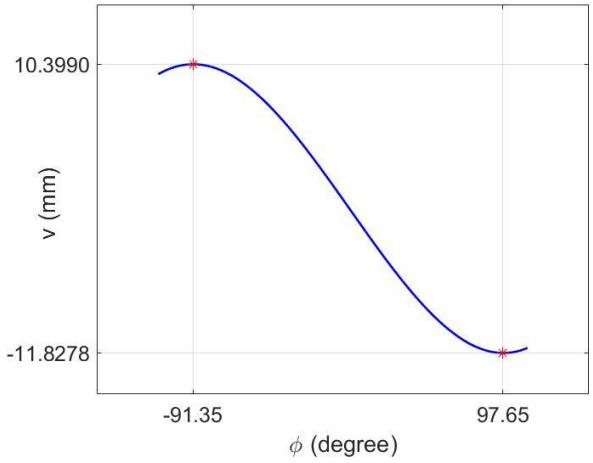

(b)

FIG. 10. Theoretical adjusting ranges in the directions of (a) horizontal and (b) vertical

Table VI. The adjusting ranges of the girder prototype

Direction	Calculated (mm)	Tested (mm)
X	-9.33~9.33	≥±8
Y	-10.67~10.46	≥±9
Z	-10.78~10.78	≥±9

B. Kinetic algorithms

The position of the girder can be described by a matrix of three rows and six columns, referring to the three coordinate positions of the six balls. The translation and rotation of the girder can be monitored by length gauges, as shown in Fig. 11. The aim of the adjusting algorithms is to transfer the adjusting magnitude of the girder to the motors' steps.

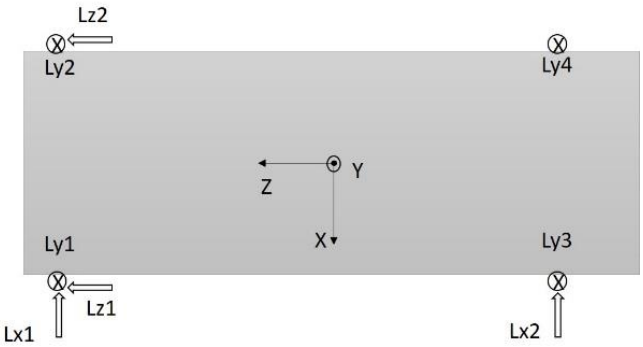

FIG. 11. Length gauges distribution

In TPS, the neighboring girder was used as the reference for the length gauges. Thus, the rotations have effect on the translations and should be eliminated first [27]. But for our prototype, the pedestals are used as references of length gauges, which can be considered motionless during short-term adjustment. So, the six DOFs have no couplings with each other.

The girder matrix of the target position G_t can be calculated by

$$G_t = R_t G_0 + T_{Tt}, \tag{4}$$

Where G_0 is the girder matrix when each ball and cam are at their origin relative positions and T_{Tt} is the translation matrixes of target position, which can be described as

$$G_0 = \begin{bmatrix} x_{10} & \cdots & x_{60} \\ y_{10} & \ddots & y_{60} \\ z_{10} & \cdots & z_{60} \end{bmatrix} \tag{5}$$

$$T_{Tt} = \begin{bmatrix} x_{Tt} & \cdots & x_{Tt} \\ y_{Tt} & \ddots & y_{Tt} \\ z_{Tt} & \cdots & z_{Tt} \end{bmatrix} \tag{6}$$

R_t is the rotation matrix of the target position. when the girder rotates with small angle, it can be simplified as

$$R_t = \begin{bmatrix} 1 & -\sigma_t & \eta_t \\ \sigma_t & 1 & -\chi_t \\ -\eta_t & \chi_t & 1 \end{bmatrix} \tag{7}$$

Similarly, the girder matrix at the current position G_c can be calculated by

$$G_c = R_c G_0 + T_{Tc}, \tag{8}$$

Then, the adjusting matrix dG can be calculated as

$$dG = G_t - G_c, \tag{9}$$

Where x_{n0}, y_{n0} and z_{n0} are the original coordinate positions of the ball labeled with number n. x_{Tt}, y_{Tt} and z_{Tt} are the translation of the girder at target position in X, Y and Z directions. χ_t, η_t, σ_t are the rotation of the girder at target position in Pitch, Yaw and Roll directions.

The calculated dG is then transferred from the assembly coordinate to the ball-cam coordinate and the adjusting angle of each shaft can be obtained. The kinetic algorithm is written in MATLAB/Simulink, while the Beckhoff controller and EtherCAT are used for control system.

C. Kinetic tests

After all the devices assembled, the open loop tests are done using all the calibrated dimensions involved as the parameters in the algorithms first, then the closed loop tests are done to verify the accuracy. The measure ranges of the length gauges are 12 millimeters, so all the kinetic tests are done in the adjusting range of ±5.3 millimeters, considering some margins.

1. Resolution and repeatability tests

The adjusting resolution is determined by the 5-phase stepping motor and the reducer with the ratio of 160. The theoretical resolution is lower than 0.8 μm without motor subdividing as shown in Fig. 12. The resolution is tested at five origin positions for all the six directions. The step size is set as 1 μm and the girder moves ten steps at each position. The resolutions and the coupling errors are both better than 1 μm and 1 μrad. The detailed results in three transition directions are shown in Table VII, which corresponds to the theoretical derivation well.

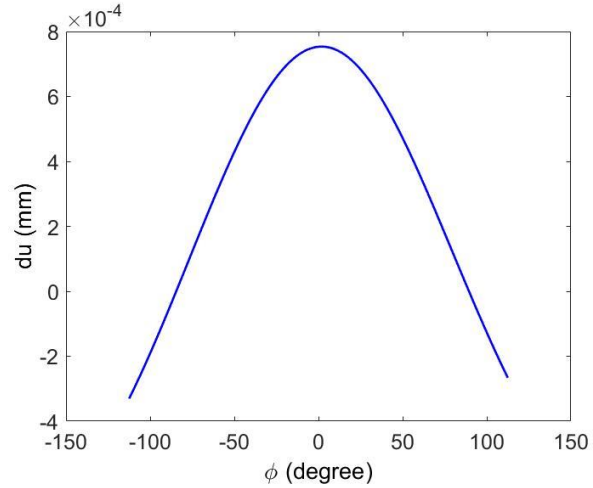

(a)

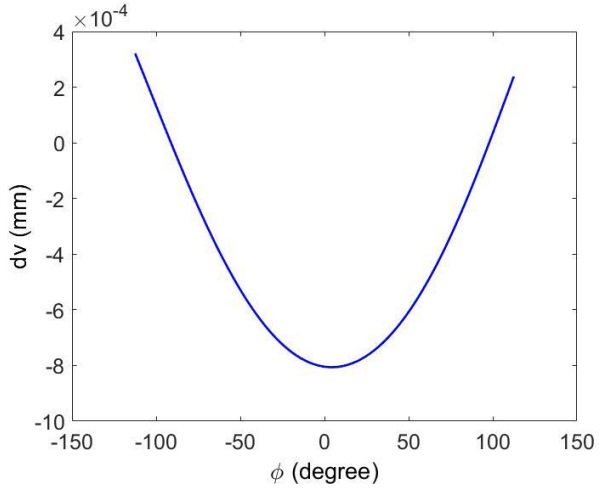

(b)

FIG. 12. The theoretical adjusting resolutions in the directions of (a) horizontal and (b) vertical

Table VII. Resolution in three transition directions

Transition direction	X	Y	Z
Girder origin positions (mm)	(-4.5 0 0)	(0 -4.5 0)	(0 0 -4.5)
	(-2.5 0 0)	(0 -2.5 0)	(0 0 -2.5)
	(0 0 0)	(0 0 0)	(0 0 0)
	(2.5 0 0)	(0 2.5 0)	(0 0 2.5)
	(4.5 0 0)	(0 4.5 0)	(0 0 4.5)
step size (μm)	1	1	1
Max absolute value of translation error (μm)	0.4	0.2	0.2
Max absolute value of coupling error (μm)	0.3	0.4	0.8

The repeatability is tested at four target positions for all the six directions. The girder moves from G_0 position to each target position G_t five times. The standard deviations are calculated to represent the repeatability, which are better than 2 μm and 2 μrad in all tested target positions. Figure 13 shows the repeatability in X-direction.

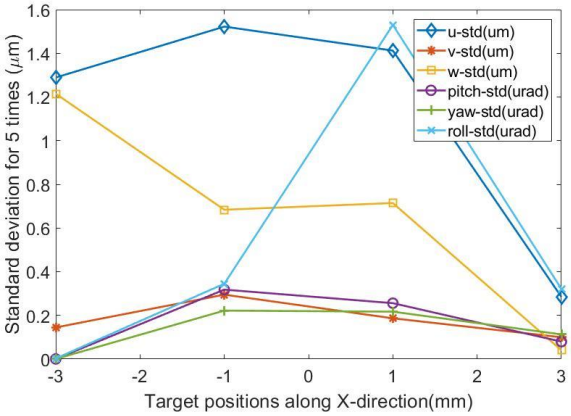

FIG. 13. Standard deviations of transitions along X-direction for 5 times

2. Adjusting error tests

As the resolution and repeatability of the prototype are good, the adjusting errors have been tested, which includes 16 target positions in each transition directions and 12 target positions in each rotation directions, as well as several target positions with both transition and rotations.

The open-loop tests are for the machining and assembling accuracy measurement, as well as the stiffness verification. The open loop errors vary with the adjusting values along particular patterns, which indicates there have some system errors. In order to affirm the error source, we add some system and random errors to each main dimension used in the algorithms. Then the adjusting errors can be back-calculated. We find that when the center to center distances of ball-cam movers (d) are modified by the deformation from gravity, the calculated adjusting errors coincide with those of the tests very well, as shown in Fig. 14. After eliminating this system error from gravity, the maximum open loop adjusting error decreases from 26 μm to 14 μm when the adjusting range is ±5 mm. This system error from gravity also verifies the stiffness validity of the ball-cam mechanism as described in sub-section III.B.

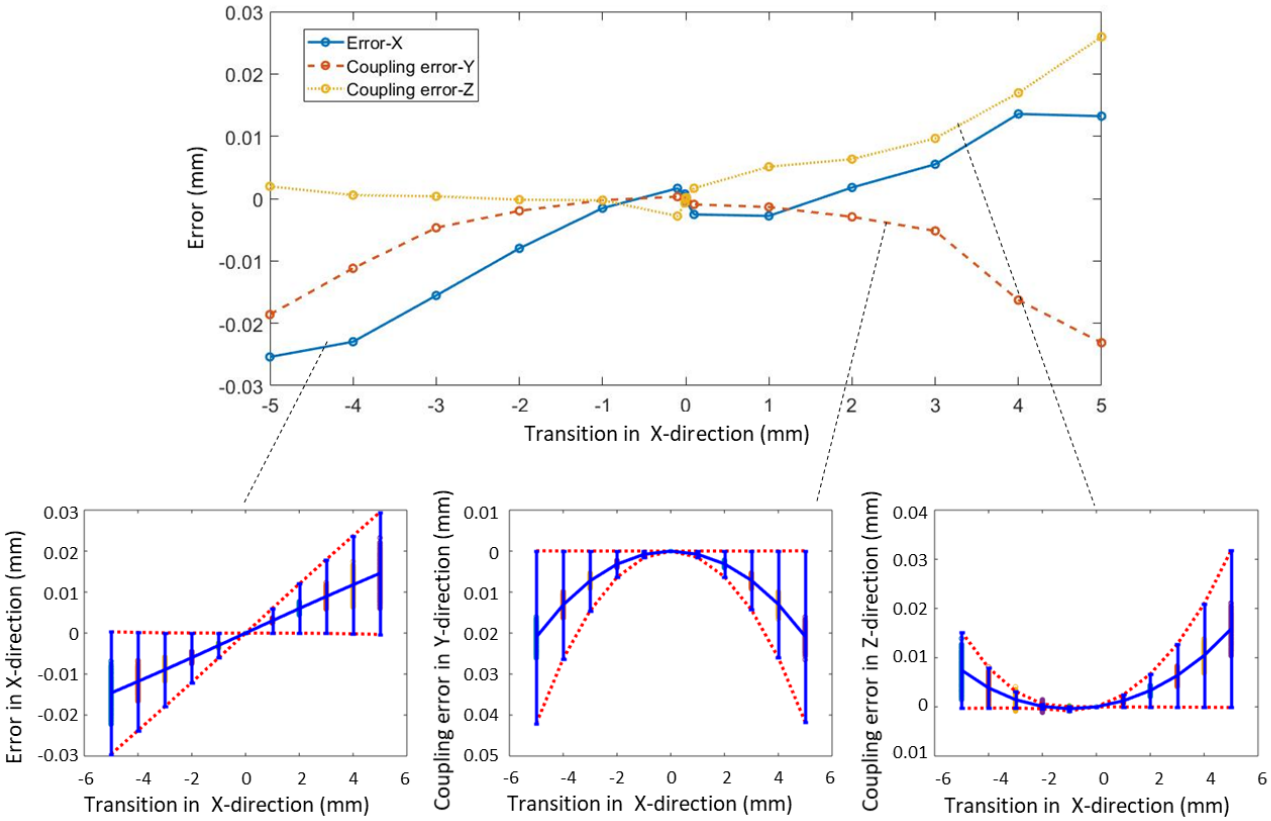

FIG. 14. The back-calculated adjusting errors with gravity and the test results (Up: tested errors with transition in X-direction; Down: back-calculated errors in each direction, the blue lines are mid-values and red lines are maximum and minimum boundaries.)

The closed loop tests are for the accuracy verification. The differential of G_t and G_c is added as the compensation values of G_t at each step, until it is decreased within the tolerance. The target positions are the same as those for open loop tests. All the adjusting errors are better than 1 μm and 5 μrad within 3 interaction times.

For all the kinetic tests above, almost all the dimension parameters in the algorithms are calibrated by coordinate measuring machine, laser tracker or other devices, which take large quantities of manpower and time. If only the positions of the length gauges are calibrated and all other dimensions use the designed values, the open loop errors will become much worse, while the closed loop errors can be remained by adding few interactions. Figure 15 shows the comparisons of the interaction number in transition along X-direction and rotation in Roll-direction. Take the former as an example, 12 target positions are set from -5 mm to 5 mm, the average interaction number for the 'calibrated dimension case' is 2.17 and that for 'designed dimension case' is 2.33. This means over 90% of calibration manpower and time can be saved only by increasing little adjusting time. This is very attractive for batch alignment.

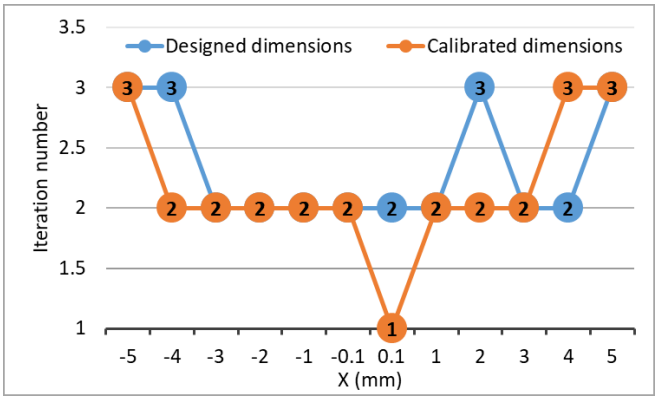

(a)

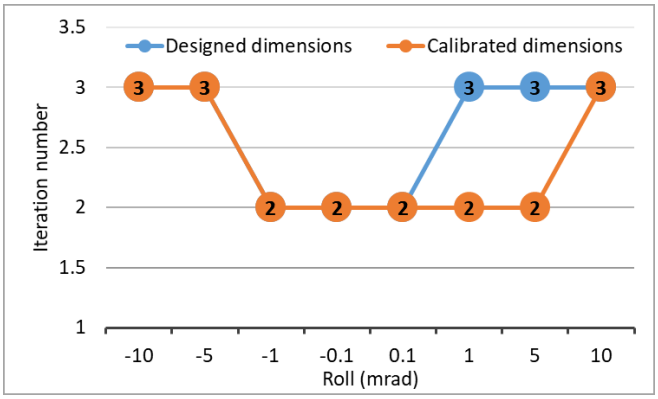

(b)

FIG. 15. The comparisons of the interactions, (a) the transition along X-direction and (b) the rotation in Roll-direction

3. Coupling error from locking system

The locking systems are used for higher stability. The girder will be locked after the adjusting process, which can bring coupling errors to the girder owing to the uneven forces in the locking process. Then the girder can be fine-tuned with the locking forces to decrease the coupling errors. In our experiment, nine target positions are tested. Each target position is repeated three times. The results demonstrate the coupling errors can be decreased better than 8 μm and 15 μrad within ten iterations. It is still much better than the alignment requirements of all the new-designed or updated photon sources. Table VIII shows one example when the target transition along Y-direction is 2.5 mm.

Table VIII. Locking and tuning process with locking system at 'Y=2.5 mm' position

		X (mm)	Y (mm)	Z (mm)	Pitch (mrad)	Yaw (mrad)	Roll (mrad)
Target position		0	2.5	0	0	0	0
Before locking		0.000	2.500	-0.001	0.000	0.000	0.000
First	Locking	0.011	2.515	0.035	-0.015	0.004	0.025
time	Tuning	0.007	2.497	-0.006	0.000	0.000	0.000
Second	Locking	0.014	2.504	-0.009	-0.014	-0.035	0.087
time	Tuning	0.004	2.499	-0.008	0.000	0.000	0.000
Third	Locking	-0.001	2.513	0.006	0.000	0.000	0.021
time	Tuning	0.001	2.507	0.004	0.000	0.000	0.015

V. CONCLUSION

A new auto-tuning magnet girder prototype has been developed and tested to pursue high stability and accuracy,

aiming at future synchrotron radiation photon sources, especially the diffraction-limited storage ring light sources. Motor driven ball-cam movers are used for the adjustment. Compared with the existing auto-tuning magnet girders, the stability and the flexibility have both been improved. Topological optimization and locking systems have been used. The stiffness of the ball-cam movers has been calculated, based on which the FEM analyses have been done. It accords to the tested results very well, from which the natural frequency of the magnet-girder assembly is deduced as high as 45.6 Hz or even higher with better fixation of the pedestals. By ingenious algorithm design and closed-loop control, plenty of calibration manpower and time can be saved by only slightly increasing the adjustment time, and the accuracy is attractive. The kinematic resolution is better than 1 μm, and the accuracy is better than 1 μm and 5 μrad within the adjusting ranges of ±5 mm without locking system, and better than 8 μm and 15 μrad after locked. The ideas and methods used in this paper demonstrate a workable direction for beam-based girder alignment, and can provide some experience for other similar problems.

ACKNOWLEDGEMENTS

This work was supported by the National Key Research and Development Program of China [2016YFA0402004]. The authors would like to thank Prof. Tse-Chuan Tseng and his study team from NSRRC for the great suggestions to push forward this work.

[1]. Eriksson, Mikael, Van Der Veen, J. Friso, and Quitmann, Christoph, Diffraction-limited Storage Rings – a Window to the Science of Tomorrow. J. Synchrotron Rad **21**, 837 (2014).

[2]. Argonne National Laboratory, Advanced Photon Source Upgrade Project Preliminary Design Report, Chapter 4: Accelerator Upgrade. APSU-2.01-RPT-002, 2017.

[3]. Yi Jiao *et.al*., The HEPS Project. J. Synchrotron Rad **25**, 1611 (2018).

[4]. Yi Jiao *et al.,* Modification and optimization of the storage ring lattice of the High Energy Photon Source. Radiat Detect Technol Methods **4**, 415–424 (2020).

[5]. V. Shiltsev, In *Proceedings of the 1995 Particle Accelerator Conference,* (IEEE, 1995)

[6]. Fang Yan *et al*., In *Proceedings of the 9th International Particle Accelerator Conference (IPAC'18), Voncouver, BC. Canada,2018,* (JACoW publishing, Geneva, 2018).

[7]. Andrey Sery and Olivier Napoly. Influence of Ground Motion on the Time Evolution of Beams in Linear Colliders. Phy. Rev. E **53**, 5323 (1996).

[8]. J. Collins *et al*., In *Proceedings of the 9th International Conference on Mechanical Engineering Design of Synchrotron Radiation Equipment and Instrumentation (MEDSI2016)*, *Spain, 2016.* (JACoW publishing, Geneva, 2016).

[9]. R. J. Leão *et al*., Poster report in International Workshop on Accelerator Alignment (IWAA'16), Grenoble, France,2016.

[10]. Filippo Cianciosi *et al*., In *Proceedings of the 9th International Conference on Mechanical Engineering Design of Synchrotron Radiation Equipment and Instrumentation (MEDSI2016)*, *Spain, 2016.* (JACoW publishing, Geneva, 2016).

[11]. Tse-Chuan Tseng. Report No. IPAC2015-thyb2.

[12]. S. Zelenika *et al*., The SLS Storage Ring Support and Alignment Systems. Nucl. Instrum. Meth. A 467-468, **99** (2001).

[13]. G. Bowden *et.al*., Precision magnet movers for the Final Focus Test Beam. Nucl. Instrum. Meth. A **368**, 579 (1996).

[14]. I.P. Martin *et.al*., In *Proceedings of the 10th European Particle Accelerator Conference (EPAC'2006), Edinburgh,Scotland,2006,* (EPS-AG, Edinburgh,Scotland, 2006).

[15]. P. Wiegand, Report No. SLS-TME-TA-2000-0145.

[16]. A. Streun *et al*., Report No. SLS-TME-TA-2001-0187.
[17]. H.S. Wang *et al*., In *Proceedings of the 13th International Conference on Accelerator and Large Experimental Physics Control Systems (ICALEPCS2011), Grenoble, France, 2011.*
[18]. W.Y. Lai *et al.,* In *Proceedings of the 3rd International Particle Accelerator Conference (IPAC'12), New Orleans, USA, 2012,* (IEEE, 2012)
[19]. Gang Xu, Yi Jiao, and Yue-Mei Peng, ESRF-type lattice design and optimization for the High Energy Photon Source. Chin. Phys. C **40**, 067004 (2016)
[20]. H Wang *et al.,* In *Proceedings of the 7th International Particle Accelerator Conference (IPAC'16)* (JACoW publishing, Geneva, 2016).
[21]. M. C. Rocha *et al.,* In *Proceedings of the 10th International Conference on Mechanical Engineering Design of Synchrotron Radiation Equipment and Instrumentation (MEDSI2018) France, 2018,* (JACoW publishing, Geneva, 2018).
[22]. Hertzian contact theory, https://www.tribonet.org/wiki/hertz-contact-theory/.
[23]. Chen Zhong, Stiffness Computation of Rolling Bearing and its Support. Coal Mine Machinery **27** (2006).
[24]. X. He, Technical report, NSRRC, 2011.
[25]. Li Chunhua *et al.,* Experimental study on magnet support plinths of advanced light source. High Power Laser and Particle Beams **33**, 034003 (2021).
[26]. Alexander H. Slocum, *Precision machine design* (A Simon & Schuster Company, Englewood Cliffs, New Jersey, 1992), p. 352.
[27]. Tse-Chuan Tseng *et al.*, In *Proceedings of the 4th International Conference on Mechanical Engineering Design of Synchrotron Radiation Equipment and Instrumentation (MEDSI2006) Japan, 2006.*